CDF/PUB/XXXX/PUBLIC/XXXX
Draft 0.0
April 13, 2006

Measurement of the Forward Backward Charge Asymmetry of di-electron pairs using the electron angular distribution

G. De Lentdecker[1], J. Lee, K. McFarland

University of Rochester, NY 14627-0171 USA

Abstract

In this note we present a measurement of the forward-backward charge asymmetry A_{FB} of electron-positron pairs resulting from the process $p\bar{p} \to Z/\gamma$ where $Z/\gamma \to e^+e^-$, using the angular distribution of the electrons. This method is an alternative to the unfolding method by matrix inversion. This measurement uses about 364 pb^{-1} of CDF Run II data.

[1] dldecker@fnal.gov

Contents

1 Introduction

The reaction $p\bar{p} \to l^+l^-$, where l is an isolated high P_T electron or muon, is mediated primarily by virtual photons at low energy [1], by the Z at $M_{l^+l^-} = M_Z$ and by the sum of the two squared amplitudes and the photon-Z interference everywhere else. The vector- and axial-vector nature of the interaction with gauge bosons gives rise to an asymmetry in the polar angle θ of the electron momentum in the rest frame of the lepton pair with respect to the proton direction. The angular asymmetry may be measured by the forward-backward charge asymmetry A_{FB}, which is defined as the following:

$$A_{FB} = \frac{\int_0^{+1} \frac{d\sigma}{d\cos\theta} d\cos\theta + \int_{-1}^{0} \frac{d\sigma}{d\cos\theta} d\cos\theta}{\int_{-1}^{+1} \frac{d\sigma}{d\cos\theta} d\cos\theta} = \frac{\sigma_F - \sigma_B}{\sigma_F + \sigma_B} \tag{1}$$

In this note we present a new method to measure the forward backward charge asymmetry of di-electron pairs using the $\cos\theta^*$ distribution. The method uses the entire angular information of the events by performing a fit to the $\cos\theta^*$ distribution and is an alternative to the unfolding method by matrix inversion described in Ref. [2] where the events are categorized as forward or backward according to the sign of $\cos\theta^*$.

This analysis is based on the same datasets and the same MC samples as the one used in Ref. [2] and both methods use the background estimation described in Ref. [3].

2 Method description

The annihilation process $f\bar{f} \to e^+e^-$ may be uniquely specified by the helicities of the initial fermion f and the final electron e^-. The corresponding scattering amplitude for the process $f\bar{f} \to e^-e^+$ can be expressed as [4]

$$\begin{aligned} A_{ij} &\equiv A(f_i\bar{f} \to e_j^- e^+) \\ &= -e_f e^2 + \frac{\hat{s}}{\hat{s} - M_Z^2 + iM_Z\Gamma_Z} C_i^Z(f) C_j^Z(e). \end{aligned} \tag{2}$$

Here $\hat{s}$ denotes the square of the center of mass energy, and the coefficients are given in Table 1 for $(i,j) = (L,R)$.
The differential cross section for $f\bar{f} \to e^-e^+$ can be written as

$$\frac{d\hat{\sigma}(f\bar{f} \to e^-e^+)}{d\cos\theta^*} = \frac{1}{8\pi\hat{s}}[(|A_{LL}|^2 + |A_{RR}|^2)(1+\cos\theta^*)^2 + (|A_{LR}|^2 + |A_{RL}|^2)(1-\cos\theta^*)^2]. \tag{3}$$

Hadronic cross section is obtained by the integral with the parton distribution functions.

	Fermion					
	u quark		d quark		Electron	
Boson	C_L	C_R	C_L	C_R	C_L	C_R
γ	$2e/3$	$2e/3$	$-e/3$	$-e/3$	$-e$	$-e$
Z	$g_Z(-\frac{1}{2}+\frac{2}{3}x)$	$g_Z(\frac{2}{3}x)$	$g_Z(\frac{1}{2}-\frac{1}{3}x)$	$g_Z(-\frac{1}{3}x)$	$g_Z(\frac{1}{2}-x)$	$g_Z(-x)$

Table 1: Left and right-handed couplings

$$\frac{\sigma(p\bar{p}\to e^+e^-)}{\cos\theta^*} = \frac{1}{3}\frac{1}{3}3\sum_{(f,\bar{f})}\int_0^1 dx_1\int_0^1 dx_2 f_f(x_1)f_{\bar{f}}(x_2)\frac{d\hat{\sigma}(f\bar{f}\to e^-e^+)}{d\cos\theta^*} \quad (4)$$

$$= \frac{1}{3}\sum_{(f,\bar{f})}\int d\tau\int dy f_f(x_1)f_{\bar{f}}(x_2)\frac{d\hat{\sigma}(f\bar{f}\to e^-e^+)}{d\cos\theta^*}, \quad (5)$$

where $\tau = M^2/s = x_1x_2$ and $(f,\bar{f})$ represents all the possible combinations of $q\bar{q}$ pair from $p\bar{p}$ collision.

We can rewrite it as a two dimensional differential cross section, $d\sigma/dM\ d\cos\theta^*$, for the production of vector boson having invariant mass M, where $M^2 = \hat{s}$. That is,

$$\frac{d\sigma}{dM\ d\cos\theta^*} = \frac{2M}{s}\frac{d}{d\tau}\left(\frac{\sigma(p\bar{p}\to e^+e^-)}{\cos\theta^*}\right) \quad (6)$$

$$= \frac{2M}{3s}\sum_{(f,\bar{f})}\frac{d\hat{\sigma}(f\bar{f}\to e^-e^+;\hat{s}=M^2)}{d\cos\theta^*}\int_{\log\sqrt{\tau}}^{-\log\sqrt{\tau}} dy f_f(x_1)f_{\bar{f}}(x_2), \quad (7)$$

where $x_{1,2} = \sqrt{\tau}e^{\pm y}$.

Eq. (7) can be re-written as :

$$\frac{d\sigma}{dM\ d\cos\theta^*} = \frac{2M}{3s}\sum_{(f,\bar{f})}\int dy f[PDF]C(\hat{s})[(|A_{LL}|^2+|A_{RR}|^2)(1+\cos\theta^*)^2 + (|A_{LR}|^2+|A_{RL}|^2)(1-\cos\theta^*)^2] \quad (8)$$

Then the 1-dim cross-section is obtained by integrating Eq.(8) over a mass range $[m_1, m_2]$:

$$d\sigma/d\cos\theta^* = \int_{m_1}^{m_2} dM\frac{d\sigma}{dM\ d\cos\theta^*}$$

$$= \frac{2}{3s}\int dy f[PDF]\sum_{(f,\bar{f})}[\int_{m_1}^{m_2} dMMC(\hat{s})(|A_{LL}|^2+|A_{RR}|^2)(1+\cos\theta^*)^2$$

$$+ \int_{m_1}^{m_2} dMMC(\hat{s})(|A_{LR}|^2+|A_{RL}|^2)(1-\cos\theta^*)^2] \quad (9)$$

That is :

$$\begin{aligned} d\sigma/d\cos\theta^* &= \frac{2}{3s}[\int dyf[PDF]\sum_{(f,\bar{f})}\int_{m_1}^{m_2} dMMC(\hat{s})(|A_{LL}|^2+|A_{RR}|^2)(1+\cos\theta^*)^2 \\ &+ \int dyf[PDF]\sum_{(f,\bar{f})}\int_{m_1}^{m_2} dMMC(\hat{s})(|A_{LR}|^2+|A_{RL}|^2)(1-\cos\theta^*)^2] \quad (10) \end{aligned}$$

which can be written as:

$$d\sigma/d\cos\theta^* = \frac{2}{3s}[A_F(1+\cos\theta^*)^2 + A_B(1-\cos\theta^*)^2] \quad (11)$$

By definition $A_{FB} = \frac{\sigma_F-\sigma_B}{\sigma_F+\sigma_B}$, and therefore $A_{FB} = \frac{3}{4}\frac{(A_F-A_B)}{(A_F+A_B)}$. Consequently, a fit to the $cos\theta^*$ distribution using Eq.(11) can be performed to measure the A_{FB} at a fixed invariant mass.
Note that method described above is true at the generator level. At the reconstruction level we have to take into account the effect of the acceptance (Acc) which varies with $cos\theta^*$ and the fit funcion becomes:

$$d\sigma/d\cos\theta^* = [C_F(1+\cos\theta^*)^2 + C_B(1-\cos\theta^*)^2] \times Acc(\cos\theta^*). \quad (12)$$

3 Monte Carlo samples

Different Monte Carlo samples have been generated for this analysis, with Pythia version 6.216 using the parton distribution function CTEQ5L. The generator includes the interference between γ^* and Z, as well as final state QED radiation. First, a large sample of 10,000,000 $Z/\gamma^* \to e^+e^-$ events with mass of $Z/\gamma^* > 30$ GeV/c^2 have been generated to calculate the acceptance and to provide a set of mutually excluding pseudo-experiments (PE), each corresponding to an integrated luminosity of 364 pb^{-1}. This sample has been generated with -1/6 X_0 less material in the plug region, which is shown to be the best estimation according to a recent study [5].

For the study of the systematic uncertainties due to the amount of material in the CDF detector two specific samples have been generated, with 1,500,000 events, each: the first sample has 1% additional material in the central tracking region at a radius of 15.0 cm; the second sample has 1/6 X_0 more material in the plug region.

Finally various Monte Carlo datasets have been used to study the backgrounds. They are summarized in Table 2.

4 Data

Although no data results are shown in this version of the note, this analysis will use the data collected by CDF between the Runs 141544 and 186598, corresponding to 364 pb^{-1}

Dataset	Process	Nbr of events	Int. Lumi (fb^{-1})
wewk5d	$WW \to ll\nu\nu$	1.6 million	1160
wewk6d	$WZ(Z \to e^+e^-)$	1/7 million	5664
hewk09	$W\gamma \to e\nu\gamma$	0.2 million	7310
atopaa	W + parton $\to e\nu + jet$	0.2 million	293
ttopkl	$t\bar{t}$ inclusive	2 millions	336

Table 2: Monte Carlo datasets used for the background estimation.

of integrated luminosity. Out of the Stream B inclusive high-p_T central electron sample, we require the Electron_Central_18 and Electron70_L2_Jet trigger paths. The events are processed with the offline production version 5.3.1 qith the calibration path 13. The analysis requires two electrons (e^- and e^+) with at least one of them in the central electromagnetic calorimeter. The selection criteria are described in section 4.1. We find 9455 events in the central-central (CC) topology and 13455 events in the central-plug (CP) topology.

4.1 Selection cuts

Central electrons are reconstructed from an energy deposit in the central electromagnetic calorimeter (CEM) where $|\eta_{det}| < 1.0$. The cuts are listed in table 3. The enrgy is corrected for the intra-tower responses and tower-to-tower gain variations. An electron is considered to be in the fiducial region of the detector if the matching track points within 60 cm in z of the center of the CDF detector and extrapolates to the calorimeter away from the wedge boundaries. The transverse momentun, p_T, of the electron is determined from the highest p_TCOT track associated with the EM cluster. The track 4-momentum is used to calculate the transverse component of the enrgy and the invariant mass of the electron pairs. The charge of the electron is determined from the curvature of the track. E_{Had}/E_{Em} is the ratio of the hadronic energy to the electromagnetic energy. E_T^{iso} is the total transverse energy within a radius of 0.4 in $\Delta R = \sqrt{\Delta\eta_{evt}^2 + \Delta\phi^2}$ of the cluster centroid, excluding the cluster energy itself. E/p is the ratio of the calorimeter energy to the momentum of the track, which deviates from 1.0 mainly because of the detector material. L_{shr} is a measure of the difference in the lateral sharing of energy among calorimeter towers, compared to test beam electron data. $|\Delta X|$ and $|\Delta Z|$ measure the distance in $r - \phi$ and z respectively between the electron shower position and the extrapolated track position.

Plug electrons are reconstructed from an energy deposit in th plug electromagnetic calorimeter (PEM) where $1.2 < |\eta_{det}| < 3.0$. The enregy is calculated from the 2×2 PEM cluster, corrected for intra-tower response variations and the PPR energy is added. Since the COT does not cover this pseudo-rapidity region, no track information is used for the plug electron selection. The z position of the PEM cluster is provided by the event primary vertex. The selection criteria are listed in Table 3. $PEM\chi^2_{3\times3}$ is

Variables	Central	Plug
E_T	$> 25GeV$	$> 25GeV$
Fiduciality	FidEle = 1 or 2	$1.18 < \|\eta\| < 3.0$
E_{Had}/E_{Em}	$< 0.055 + 0.00045 * E$	$< 0.05 + 0.026 * log(E/100)$
E_T^{iso}	$< 3 + 0.02 \times E_T$	$< 1.6 + 0.02 \times E_T$
p_T	> 15 GeV ($E_T < 100$ GeV) > 25 GeV ($E_T > 100$ GeV)	N/A N/A
E/p	$< 2.5 + 0.015 \times E_T$ ($E_T < 100$ GeV)	N/A
track$\|z_0\|$	$< 60cm$	N/A
L_{shr}	< 0.2	N/A
$\|\Delta X\|$	$< 3cm$	N/A
$\|\Delta Z\|$	$< 5cm$	N/A
$PEM\chi^2_{3\times3}$	N/A	< 25

Table 3: Identification cuts applied to the electron candidates in this analysis.

	Data	MC
Central	1.000	0.997
Plug	1.029 (West) 1.033 (East)	1.013

Table 4: Energy scale factors for the data and the MC.

calculated from the comparison of the energy distribution in 3×3 PEM towers around the seed tower to distributions from test beam data.

4.2 Electron energy scale and resolution

The global energy scale of the electrons in the central and plug regions is adjusted so that the spectrum agrees with the prediction from M_Z as measured by LEP I. This adjustment procedure is described in Ref [6]. The histograms of the di-electron pair invariant mass distribution, with a bin size of 1 GeV/c^2, are fitted to a Gaussian function in the range $86 < M_{ee} < 98$ GeV/c^2. The global energy scale factors for central and plug electrons are given in Table 4. The Gaussian widths are given in Table 5.

In order to match the width of CP events in the data and MC, the plug electron energy has been varied randomly. Since the width of the CC events is smaller than with the data, we did not add extra smearing to the central electrons. The correction are re-calculated for the samples with extra-material used to study the sytematics uncertainties due to the detector material.

	Before correction		After correction	
	Data	MC	Data	MC
CC	2.988	3.072	2.988	3.030
CP West	3.008	2.934	2.971	2.972
CP East	3.174	2.928	3.072	3.082

Table 5: Gaussian widths for the data and the MC in GeV/c^2, before and after the correction.

Dataset	Process	$\sigma\times$ Br (pb)	CC	CP	Total
wewk5d	$WW \to ll\nu\nu$	1.39	5.9	6.5	12.4±0.3
wewk6d	WZ $(Z \to e^+e^-)$	0.41	5.6	6.4	12.0±0.3
hewk09	$W\gamma \to e\nu\gamma$	27.2	0.7	25.3	26.1±1.5
atopaa	$W+$ parton $\to e\nu + jet$	682.4	7.5	29.2	36.6±6.9
ttopkl	$t\bar{t}$ inclusive	5.50	3.2	1.9	5.1±0.2

Table 6: Numbers of EWK background estimated from MC.

5 Backgrounds

5.1 Jet background

The dominant background in this analysis is the background of jets misidentified as electrons. This background has been estimated using the extrapolation method described in Ref [3]. The di-jet background from QCD processes is estimated with this method. Note that the process $W + jet \to e\nu + jets$ also involves a misidentified jet. Since this background presents one electron and one jet in the final state, the background estimation returns only a part of the total background. Therefore the $W + jet$ contribution is subtracted from the isolation extrapolation result and the $W + jet$ background contribution is estimated from MC.

To measure the A_{FB} in the data, the shape of the di-jet background also needs to be described as a function of the invariant mass and $\cos\theta^*$. The di-jet background prediction, function of M_{ee} and $\cos\theta^*$ is added to the fit function (Eq.(12)).

5.2 Other backgrounds

All the other backgrounds that do not involve a misidentified jet are estimated from MC. Such backgrounds include di-boson production and $t\bar{t}$ events. $W+jet$, which is an exception (see section 5.1), is also estimaed from the MC. Table 6 shows the dataset, the cross-section and the estimated number of events of each background process.

(Note that at this stage we have not yet included those background in the background prediction to make the fit of the $\cos\theta^*$ distribution.)

Bin	Mass Range (GeV/c^2)	Aver. A_{FB}	Aver. Stat. Err.
1	$50 < M < 65$	-0.284	0.101
2	$65 < M < 76$	-0.454	0.042
3	$76 < M < 82$	-0.334	0.033
4	$82 < M < 88$	-0.125	0.016
5	$88 < M < 94$	0.064	0.009
6	$94 < M < 100$	0.215	0.017
7	$100 < M < 106$	0.382	0.040
8	$106 < M < 120$	0.486	0.040
9	$120 < M < 140$	0.580	0.046
10	$140 < M < 200$	0.617	0.043
11	$200 < M < 300$	0.576	0.086
12	$300 < M < 600$	0.615	0.150

Table 7: Average A_{FB} of 11 pseudo-experiments with the average statistical errors in 12 invariant mass bins.

6 A_{FB} measurement

6.1 Pseudo-experiments

From the large sample of 10,000,000 $Z/\gamma^* \rightarrow e^+e^-$ events, 11 mutually exclusive pseudo-experiments have been thrown.Each pseudo-experiment corresponds to an integrated luminosity of 364 pb^{-1}. To each pseudo-experiment we fit the fit the $\cos\theta^*$ distribution in 12 invariant mass bins, using the fit function shown in Eq. 12. The results of the 11 pseudo-experiments are averaged and shown in Table 7 and in Figure 1a). Figure 1b) shows the average of the difference between the pseudo-experiment A_{FB} and the A_{FB} predicted by the SM at Leading Order (LO). The error bars represent the average of the statistical error of the 11 pseudo-experiments.

7 Systematic uncertainties

7.1 Energy scale and energy resolution

The uncertainty of the energy scale is estimated from the variation of the position on the Gaussian peak of the invariant mass as a functiom of $|\eta_{det}|$ of the electron. Based on the distribution of the masses corresponding to the peak, the energy scale is varied by pm 0.2 % in the region $|\eta_{det}| < 2.35$ and by pm 0.8 % for $|\eta_{det}| > 2.35$. Similarly the uncertainty on the enrgt resolution is found from variation of the width of the Gaussian as a fucntion of $|\eta_{det}|$. The resolution has been modified in order to increase the width

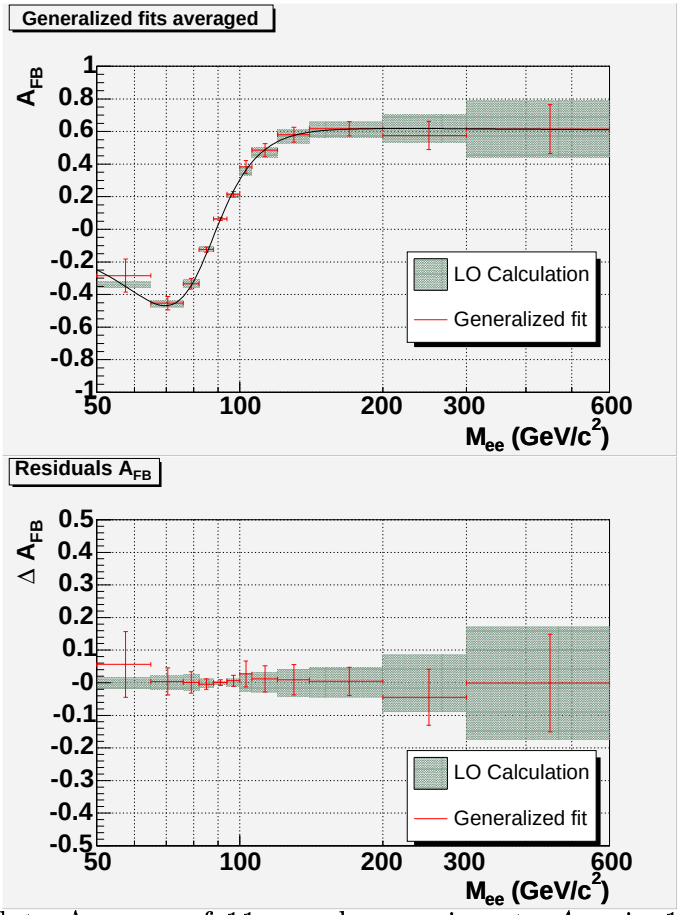

Figure 1: Upper plot: Average of 11 pseudo-experiments A_{FB} in 12 invariant mass bins. The shaded area represents the LO prediction with the expected spread of the measurement for 364 pb^{-1}. Lower plot: difference between the pseudo-experiment A_{FB} and the LO SM A_{FB}. The error bars represent the average of the statistical error of the 11 pseudo-experiments.

by 0.3 GeV in the central region, by 0.2 GeV in the West plug and by 0.4 GeV in the East plug. These effects are applied to the 11 pseudo-experiments then the fit to the $\cos\theta^*$ distributions applied to obtain A_{FB}. The shift in A_{FB} with respect to the value obtained without modifying the energy scale and energy resolution is averaged over the 11 pseudo-experiments, which provides the systematic uncertainty on the A_{FB} measurement from the energy scale and energy resolution. The average values of the A_{FB} shifts are shown in Table 8 for the energy scale and energy resolution. Figure 2 (upper) shows the average of the shifts in A_{FB} when we vary the energy scale up (blue) and down (red). Figure 2 (lower) shows the average of the shifts in A_{FB} when we vary the energy resolution. The errors bars correspond to the RMS of the shifts distribution divided by square root of (number of pseudo-experiments - 1).

Bin	Mass Range (GeV/c^2)	Scale up	Scale down	Width
1	$50 < M < 65$	-0.012	0.003	0.012
2	$65 < M < 76$	-0.007	0.003	0.004
3	$76 < M < 82$	0.002	0.011	0.014
4	$82 < M < 88$	-0.005	0.001	0.004
5	$88 < M < 94$	-0.002	0.002	0.000
6	$94 < M < 100$	-0.005	0.007	-0.006
7	$100 < M < 106$	-0.002	0.003	-0.032
8	$106 < M < 120$	-0.000	0.004	0.004
9	$120 < M < 140$	-0.003	-0.006	-0.001
10	$140 < M < 200$	0.002	0.006	0.004
11	$200 < M < 300$	0.000	-0.003	-0.017
12	$300 < M < 600$	0.000	0.000	0.019

Table 8: Energy scale and energy resolution systematics.

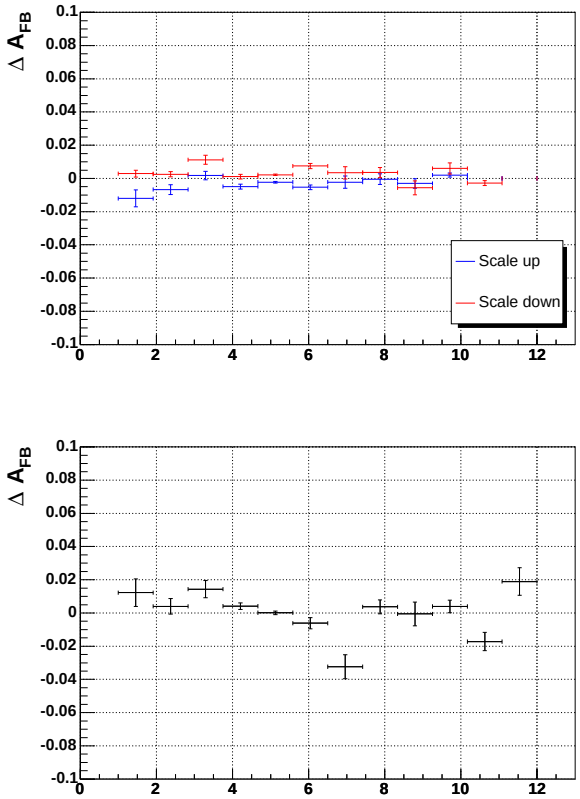

Figure 2: Upper plot: effect of the energy scale-up (blue) -down (red) on A_{FB}. Lower plot: effect the energy resolution on A_{FB}.

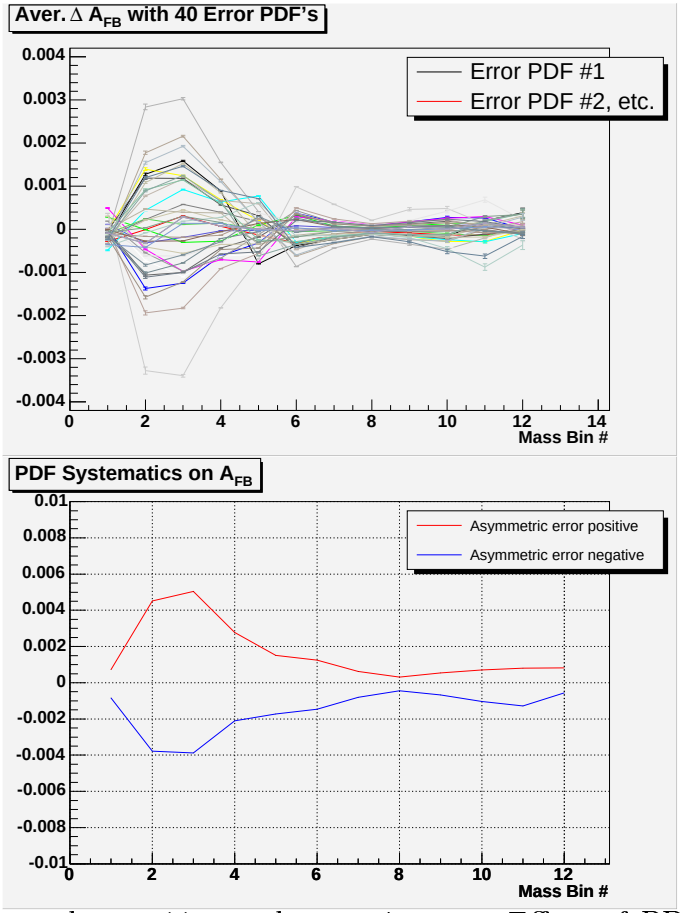

Figure 3: A_{FB} averaged over 11 pseudo-experiments. Effect of PDF's: the 40 sets (above) the summed uncertainties (bottom) (not redone).

7.2 PDF uncertainty

The acceptance has been computed for the 40 error CTEQ6M PDF's by reweighting the events. The A_{FB} fit has been performed for the 11 pseudo-experiments with each of the 40 acceptance. Figure 3 shows the average of the shift of A_{FB}, averaged over the 11 pseudo-experiments, for each of the 40 error PDF's (upper plot). The lower plot of figure 3 shows the shifts of the 40 error PDF's combined according to the CDF prescription. This combination results in a positive and negative error listed in Table 9.

7.3 Material systematics

To estimate the systematic uncertainty on the A_{FB} measurement due to the detector material, we have simulated two samples of $Z/\gamma^* \rightarrow e^+e^-$ events with two different amount of material. One contains 1 % X_0 extra material in the central tracking region and the other contains 1/6 X_0 extra material in the plug region. The acceptance has been computed for both samples and used in the fit to the $\cos\theta^*$ distributions of

Bin	Mass Range (GeV/c^2)	Pos. uncert.	Neg. uncert.
1	$50 < M < 65$	0.001	-0.001
2	$65 < M < 76$	0.005	-0.004
3	$76 < M < 82$	0.005	-0.004
4	$82 < M < 88$	0.003	-0.002
5	$88 < M < 94$	0.002	-0.002
6	$94 < M < 100$	0.001	-0.001
7	$100 < M < 106$	0.001	-0.001
8	$106 < M < 120$	0.000	-0.000
9	$120 < M < 140$	0.001	-0.001
10	$140 < M < 200$	0.001	-0.001
11	$200 < M < 300$	0.001	-0.001
12	$300 < M < 600$	0.001	-0.001

Table 9: The 40 PDF shifts combined.

the 11 pseudo-experiments. Table 10 shows the shifts in A_{FB} when extra material is added with respect to the A_{FB} measured without extra material; the shifts of the 11 pseudo-experiments are averaged. The central and plug extra material uncertainties are added in quadrature to obtain the total material systematic uncertainty on the A_{FB} measurement.

7.4 Background systematics

The uncertainty in the amount of background may change the measurement of A_{FB}. To estimate the systematic uncertainty due to the background we varied by $\pm 1\sigma$ the amount of background and measured the efect on the A_{FB}. The average of the A_{FB} shifts are given in Table 11.

7.5 NLO QCD corrections

Since NLO QCD processes may modify the angular distribution of the electron with respect to the LO angular distribution we have estimated the systematic uncertainties due to the NLO QCD processes. The events of the pseudo-experiments have been weighted using the NLO/LO K-factor as a function of the invariant mass and $\cos\theta^*$ [7]. Such K-factor is shown as a function of $\cos\theta^*$ for various invariant masses in figure 4. The shifts of A_{FB} averaged over the 11 pseudo-experiments are given in Table 12.

Bin	Mass Range (GeV/c^2)	Central	Plug	Total
1	$50 < M < 65$	0.045	0.058	0.073
2	$65 < M < 76$	0.005	0.073	0.073
3	$76 < M < 82$	0.002	0.007	0.007
4	$82 < M < 88$	0.001	0.005	0.005
5	$88 < M < 94$	0.002	0.002	0.002
6	$94 < M < 100$	0.013	0.003	0.013
7	$100 < M < 106$	0.024	0.031	0.039
8	$106 < M < 120$	0.003	0.019	0.019
9	$120 < M < 140$	0.036	0.022	0.043
10	$140 < M < 200$	0.004	0.010	0.011
11	$200 < M < 300$	0.032	0.008	0.033
12	$300 < M < 600$	0.029	0.022	0.036

Table 10: Average of the shifts in A_{FB} when extra material is added independently in the central region and in the plug region. Both systematics are added in quadrature to obtain the total material systematics on A_{FB}.

Bin	Mass Range (GeV/c^2)	Bkgd up	Bkgd down
1	$50 < M < 65$	-0.002	0.006
2	$65 < M < 76$	0.000	0.003
3	$76 < M < 82$	0.000	0.001
4	$82 < M < 88$	-0.000	-0.000
5	$88 < M < 94$	0.000	-0.000
6	$94 < M < 100$	-0.000	-0.000
7	$100 < M < 106$	0.000	-0.000
8	$106 < M < 120$	-0.006	-0.001
9	$120 < M < 140$	-0.007	-0.007
10	$140 < M < 200$	-0.010	-0.007
11	$200 < M < 300$	-0.018	-0.013
12	$300 < M < 600$	-0.018	0.001

Table 11: Averaged shifts in A_{FB} when the number of background events is varied by $+1\sigma$ and -1σ.

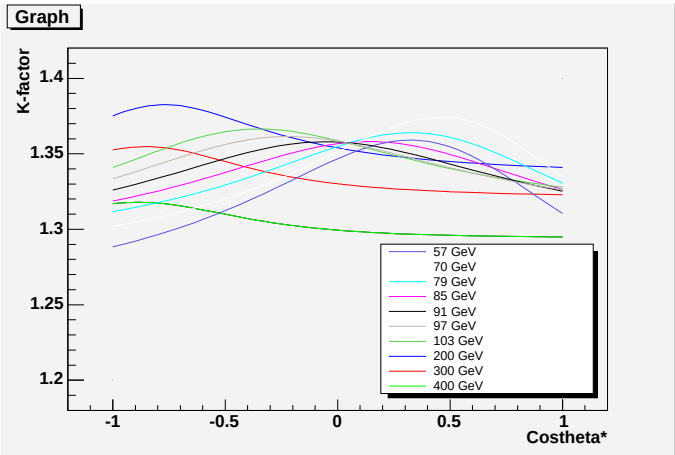

Figure 4: K-factor has a function of $\cos\theta^*$ for different invariant masses [7].

Bin	Mass Range (GeV/c^2)	NLO syst
1	$50 < M < 65$	-0.012
2	$65 < M < 76$	-0.012
3	$76 < M < 82$	-0.007
4	$82 < M < 88$	-0.002
5	$88 < M < 94$	0.002
6	$94 < M < 100$	0.005
7	$100 < M < 106$	0.006
8	$106 < M < 120$	0.005
9	$120 < M < 140$	0.006
10	$140 < M < 200$	0.005
11	$200 < M < 300$	0.004
12	$300 < M < 600$	0.002

Table 12: Systematic error on A_{FB} due to the NLO QCD corrections.

8 Uncertainties summary

Table 13 summaries all the uncertainties, statistical and systematics, on the A_{FB} measurement. The total uncertainty is obtained by adding in quadrature the statistical and the total systematic uncertainties. A_{FB} is the average of the 11 pseudo-experiment measurements.

Mass Range (GeV/c^2)	A_{FB}	Stat	E scale	Width	PDF	Mat	BG	NLO	Syst	Total
$50 < M < 65$	-0.284	0.101	0.012	0.012	0.001	0.073	0.006	0.012	0.077	0.127
$65 < M < 76$	-0.454	0.042	0.007	0.004	0.005	0.073	0.003	0.012	0.074	0.085
$76 < M < 82$	-0.334	0.033	0.011	0.014	0.005	0.007	0.001	0.007	0.021	0.039
$82 < M < 88$	-0.125	0.016	0.005	0.004	0.003	0.005	0.000	0.002	0.009	0.018
$88 < M < 94$	0.064	0.009	0.002	0.000	0.002	0.002	0.000	0.002	0.004	0.010
$94 < M < 100$	0.215	0.017	0.007	0.006	0.001	0.013	0.000	0.005	0.017	0.024
$100 < M < 106$	0.382	0.040	0.003	0.032	0.001	0.039	0.000	0.006	0.051	0.065
$106 < M < 120$	0.486	0.040	0.004	0.004	0.000	0.019	0.006	0.005	0.021	0.045
$120 < M < 140$	0.580	0.046	0.006	0.001	0.001	0.043	0.007	0.006	0.044	0.064
$140 < M < 200$	0.617	0.043	0.006	0.004	0.001	0.011	0.010	0.005	0.017	0.046
$200 < M < 300$	0.576	0.086	0.003	0.017	0.001	0.033	0.018	0.004	0.042	0.096
$300 < M < 600$	0.615	0.150	0.000	0.019	0.001	0.036	0.018	0.002	0.045	0.156

Table 13: Summary of all the uncertainties: statistical and systematic. A_{FB} is the average of the 11 pseudo-experiment measurements. The total uncertainty is obtained by adding in quadrature the statistical uncertainty and the total systematic uncertainty.

9 Conclusion

In this note we present a new method to measure the forward backward charge asymmetry of di-electron pairs using the $\cos\theta^*$ distribution. This method is an alternative to the unfolding method described in Ref. [2] where the events are categorized as forward or backward according to the sign of $\cos\theta^*$.

The scope of this note is currently limited to the presentation of our analysis method and the estimation of its performance. We present the expected statistical uncertainty and the systematic uncertainties using pseudo-experiments. The systematic effects of the energy scale, energy resolution, material, PDF's, background and NLO QCD corrections have been estimated.

References

[1] S.D. Drell and T.-M. Yan, Phys Rev. Lett. 25, 316, 902 (E) 1970; Ann. Phys. (N.Y.) 66, 578 (1971). 3

[2] J. Lee et al., CDF Note 7998. 3, 16

[3] J. Lee et al., CDF Note 7997. 3, 8

[4] J.L. Rosner,*Phys. Rev.* **D 54** (1996) 1078, hep-ph/9612299. 3

[5] G. Chiarelli et al., CDF Note 8036. 5

[6] S. Haper et al., CDF Note 7687. 7

[7] P. Mathews et al., hep-ph/0507250. 13, 15